Evaporative capillary rise

Jungtaek Kim [●],[1] Yeonsu Jung [●],[2] and Ho-Young Kim [●][1,*]

[1]*Department of Mechanical Engineering, Seoul National University, Seoul 08826, Korea*
[2]*School of Engineering and Applied Sciences, Harvard University, Cambridge, Massachusetts 02138, USA*

The capillary rise in vertically situated open microchannels can be severely limited by liquid evaporation. Here we quantitatively study the rise dynamics using a combination of experiment and theory. On evaluating the effects of the enhanced evaporation near the solid-liquid-gas contact line on the mass transfer rate from liquid in a microchannel, we set up a differential equation for the temporal evolution of rise height by considering mass conservation of evaporating viscous liquid drawn against gravity via capillarity. It is found that there exists an optimal channel width that maximizes the equilibrium rise height under a given channel depth, unlike nonevaporative rise whose equilibrium height monotonically increases with the reduction of channel width. Our work can lay a foundation for understanding the evaporative capillary rise dynamics occurring in various porous media of biological, natural, and artificial settings.

The rise of a liquid against gravity through small voids of porous media is one of the clearest manifestations of capillarity. The surface tension drives the flow by generating a pressure jump across the liquid-gas interface, the Laplace pressure, which is inversely proportional to the void size [1]. Water rises through a vertical glass tube of submillimetric diameter to a great distance (~10 cm) from a reservoir. But we mundanely observe water wet a sheet of paper only a few centimeters above the reservoir although the pore size of paper is far smaller than the usual tube diameter. It is because the capillary flow is limited by evaporation of water from the pores open to the atmosphere. Although such evaporation-limited flows are frequently observed or utilized in heat pipes [2], desalination [3], evaporation-assisted pumping [4], hygroscopic actuation [5], and nanoparticle assembly [6], the understanding of capillary rise dynamics undergoing evaporation is still far from complete. The rise height evolutions within porous media including metallic weaves [7] and knitted fabrics [8] were experimentally measured to be severely affected by evaporation. Such rise dynamics in porous media considering capillarity, gravity, and evaporation were theoretically analyzed by assuming evaporative flux values from the wet porous surface [9,10]. It was hard to obtain satisfactory agreements of theoretical and experimental results in the evaporative capillary rise dynamics, mainly because of insufficient knowledge of the evaporative flux from the wet pores. Here we study the capillary rise dynamics affected by evaporation through adopting a simple but fundamental model system where the evaporative flux can be both accurately measured and theoretically analyzed. The model system consists of vertical open hydrophilic channels as shown in Figs. 1(a) and 1(b).

Incorporating the effects of evaporation in the rise dynamics is by no means simple within microchannels because the evaporative flux per unit interfacial area depends on the distance from the liquid-gas-solid three phase contact line rather than being a constant [11]. Thus, we begin with

---

*hyk@snu.ac.kr

L032001-1
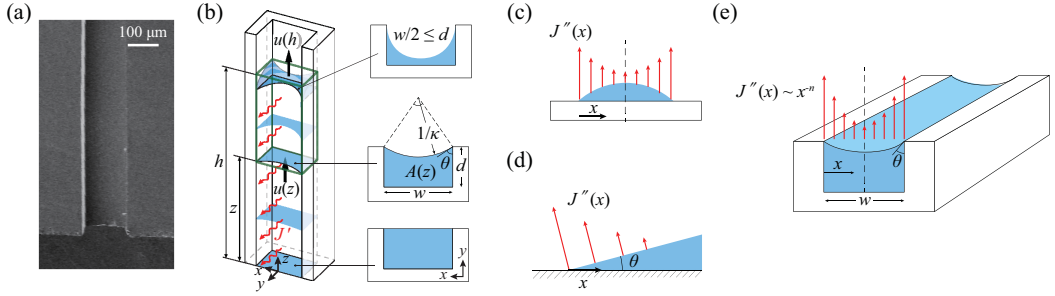
FIG. 1. (a) An open channel on a Si wafer, 144 μm wide and 94 μm deep. (b) The cross sections of a liquid column rising through a vertical open channel. (c) Evaporation of a liquid drop on a flat solid surface. (d) A wedge-shaped meniscus undergoing evaporation. (e) Evaporation of a meniscus straddling the corners of a rectangular channel of width w.

analyzing the evaporative flux from liquid meniscus taking into account the effects of the contact line. Then we theoretically predict the rate of capillary rise in open channels and experimentally corroborate them. We finally find the optimal channel width to exist that maximizes the equilibrium rise height, where the capillary effects are balanced with those by gravity and evaporation.

Evaporation from an open capillary channel occurs in close proximity to three-phase contact lines, which complicates the evaluation of the evaporative mass flux. For a liquid drop sitting on a wettable solid, Fig. 1(c), it is now well established that evaporative mass transfer is enhanced near the contact line, which is responsible for the so-called coffee ring stains of drying suspensions [12]. The evaporative volume flux per unit area from a liquid surface to the atmosphere, J'' is given by Ficks law, $J'' = -D\partial c/\partial n$, where D is the diffusivity of vapor in the air and $\partial c/\partial n$ is the gradient of vapor concentration c in the normal direction to the surface. Solving the steady-state concentration equation, $\nabla^2 c = 0$, in the surroundings of a wedge-shaped meniscus on a flat solid surface as shown in Fig. 1(d), we find $J''(x) = j_0 x^{-(\pi/2-\theta)/(\pi-\theta)}$ with x and θ respectively being the distance from the contact line and the contact angle [12]. The coefficient, j_0 depends on the vapor diffusivity and density, the far-field and saturation concentrations [13–15]. The divergent nature of the flux near the contact line as $x \to 0$ is roughly attributed to geometric singularity where the sharp edge encounters a wide open atmosphere [16]. Then we expect similar singularity for a meniscus straddling the corners of channels as shown in Fig. 1(e), which leads us to write $J'' \sim x^{-n}$ with $0 < n < 1$. Here $\sim$ signifies "is scaled as."

The evaporative volume flux per unit length of channel of width w is estimated as $J' \approx 2\int_0^{w/2} J''(x)dx$, where the evaporation near the contact line ($x \to 0$) is assumed to dominate over that in the center of channels of submillimetric width. When the width of channel exceeds $\sim$10 mm, evaporation from bulk region dominates over the contact line effect, so that J'' is almost constant or J' is proportional to w (Supplementary Material A [17]). We thus anticipate $J' = J_0 w^{(1-n)}$ for narrow channels where significant capillary rise can be observed. Complicated geometry involving channel corners and curved meniscus, which hardly allows analytical solutions, led us to numerically solve the Laplace equation for c, $\nabla^2 c = 0$, in the atmosphere and find J'' while varying the contact angle and the channel width. As delineated in Supplementary Material A, we find that J_0 and n are nearly constant regardless of the contact angle.

To corroborate the theoretical prediction, we measured the evaporative flux of ethanol from an open channel using an experimental setup illustrated in Fig. 2(a). Ten identical rectangular microchannels of 20-mm length were formed in parallel on a Si wafer using the deep reactive ion etching process. The ends of the channels were connected to a separate liquid reservoir through flexible tubes. The Si surface is highly wettable by ethanol, and thus the equilibrium contact angle, θ_e is nearly zero. As ethanol evaporated from the initially filled channels, the liquid was continuously
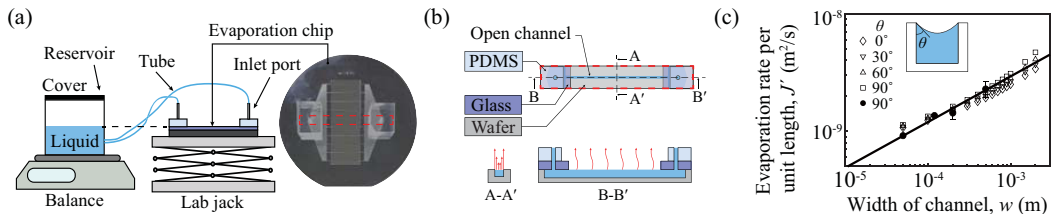
FIG. 2. (a) Experimental setup to measure the evaporative flux from the interface of ethanol, which fills 10 identical horizontal channels of the width w. The liquid is supplied from the reservoir to the channels through flexible tubes, which are coupled with the channels by the rigid tubes and through-holes of the end walls made of PDMS and glass. (b) Schematics of a single channel from which liquid evaporates. (c) Comparison of experimentally measured (filled symbols) and numerically computed (empty symbols) values of evaporation rate per unit length, J' versus the channel width for different contact angles. The solid line corresponds to $J' = J_0 w^{(1-n)}$, as determined by the least square method with the coefficient of determination $R^2 = 0.9712$. Each experimental data point corresponds to the average of five measurements.

fed from the reservoir whose liquid level was initially set to match the height of the channels as shown in Fig. 2(b). The weight decrease of the reservoir was measured by an electronic balance (Mettler Toledo ML204T), which allowed us to obtain the evaporative flux. The channel width ranged from 50 to 500 μm. The temperature and relative humidity of the surrounding air were respectively maintained at 20 °C and 20%.

The measured rate of mass decrement was divided by the ethanol density (789 kg m^{-3}) and the entire length of channel exposed to air (200 mm total for 10 channels) to find the evaporation rate of ethanol per unit length, J' versus channel width, as shown in Fig. 2(c). The data agree with the numerically computed J' for different contact angles (numerical details in Supplementary Material A [17]), which allows us to write $J' = J_0 w^{(1-n)}$ with $n = 0.62$ and $J_0 = 4.1 \times 10^{-8}$ m^{1+n} s^{-1}. The positive value of n signifies that J' does not decrease linearly with the reduction of channel width (as in large channels with constant J'') but rather depends weakly on w owing to the enhanced evaporation near the contact line.

Based on the quantitative measurement of evaporation flux from filled horizontal open microchannels, we now model the dynamics of evaporative capillary rise of a wetting liquid through an initially dry vertical open channel as shown in Fig. 1(a). The liquid rise velocity is determined by the mass conservation considering the upward flow affected by capillarity, gravity and viscosity, and the loss due to evaporation. For a control volume involving the advancing liquid-air interface, a green cuboid in Fig. 1(b), we write

$$A(z)u(z) - (h - z)J' = A(h)\dot{h}, \tag{1}$$

where $A(z)$ and $u(z)$ are respectively the cross-sectional area of the liquid column and the average velocity at the elevation z from the reservoir and $\dot{h} = dh/dt$. In the following, we obtain h, the capillary rise height, as a function of time t by solving Eq. (1). Here we considered the evaporative flux from the side area only while neglecting that from the top surface, whose extension from the bulk is discussed in detail below.

The cross-sectional area of liquid column at z is determined by the meniscus curvature $\kappa(z)$ as shown in Fig. 1(b): $A(z) = w\text{d} - (w/2)^2[(\pi/2 - \theta)/\cos^2\theta - \tan\theta]$, where d is the channel depth. The angle of the pinned meniscus at the channel edges, θ, is given by $\theta(z) = \cos^{-1}(w\kappa/2) < \pi/2$. We assume a fully developed flow because $\text{Re}(\text{d}/h) \ll 1$ except for the extremely early stages, where the Reynolds number $\text{Re} = U\text{d}/\nu$ with U and ν respectively being the characteristic flow velocity and the kinematic viscosity. Then the pressure in the liquid column decreases linearly from the atmospheric pressure p_a at $z = 0$ to $p_a - \gamma\kappa_t$ at $z = h(t)$, where γ is the surface tension coefficient of liquid.
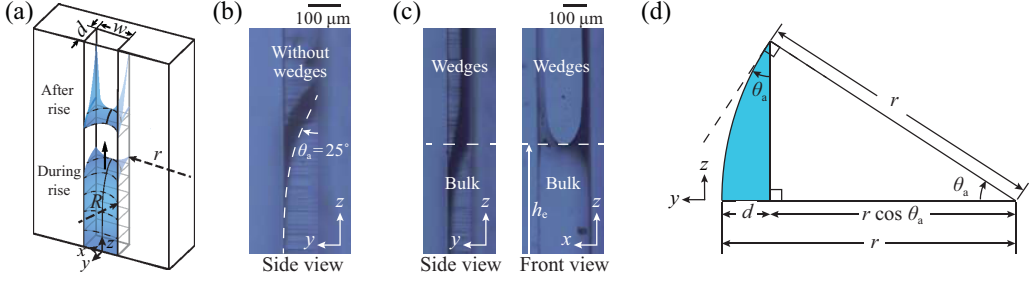
FIG. 3. (a) Schematics of top menisci during and after capillary rise in an open channel. The radii of curvature in the x-y and y-z plane are denoted as R and r, respectively. (b) Side view image of a meniscus during rise in a partially wettable channel, where a dotted line indicates a convex (in the y-z plane) meniscus with the advancing contact angle of $\theta_a = 25°$. (c) Side and front view images of a meniscus after the equilibrium rise height has been reached. (d) Radius of curvature of the convex meniscus. The transparent PDMS channel has the width and depth of $w = 200$ μm and d $= 100$ μm.

Near the top of the rising liquid column, the liquid can no longer be pinned at the channel edges and its interface touches the channel bottom at the advancing contact angle of θ_a, as illustrated in Fig. 3. While the meniscus is concave in the x-y plane, it is convex in the y-z plane. To clearly visualize the top meniscus, we carried out additional experiments using an open channel made of transparent polydimethylsiloxane (PDMS), and the result is shown in Fig. 3(b). The equilibrium contact angle of ethanol on PDMS is $20°$, and thus the advancing contact angle θ_a on PDMS is also greater than on the highly wettable Si surface. As drawn in Fig. 3(d), the radius of curvature r of the convex curve in the y-z plane is found as a function of the channel depth d and θ_a: $r = $ d$/(1 - \cos\theta_a)$. On highly wettable surfaces, θ_a is fairly small, so that $r \gg$ d. For deep channels (d $\geqslant w/2$), r is much greater than the radius of curvature in the x-y plane. The experimental image in Fig. 3(b) using the partially wettable surface shows $\theta_a = 25°$ and the corresponding $r = 1$ mm, which is much greater than the half channel width, $w/2 = 0.1$ mm. For highly wettable surfaces like Si, θ_a is even smaller, leading to $r \gg w/2$. Therefore, the additional curvature in the y-z plane has negligible effects on the mean curvature of the top surface ($\kappa_t \gg r^{-1}$) on highly wettable channels. Furthermore, the additional rise height ($r \sin\theta_a$) and area ($wr\theta_a$) due to the convex meniscus are far smaller than the equilibrium rise height (h_e) and side area of liquid column (wh_e) in Si channels.

After the bulk liquid column reached its equilibrium height, the channel corners were additionally wetted by the liquid, as shown in Fig. 3(c). This corner meniscus forms because the sharp corners with a high surface energy can locally draw liquid upward. In our experiments with Si channels, the corner menisci of the ethanol were observed to extend up to approximately 1 mm, which was insignificant compared to the typical equilibrium bulk rise height ranging from 10 to 50 mm. When the channels were shallow such that d $< w/2$, the similar liquid wedges were experimentally found to rise along the channel edges from the early stages, dominating over the bulk rise. The understanding of the corner flows of wedges needs a separate theoretical consideration [18] and is not treated here. We only deal with deep channels in this work.

For deep channels, as the pressure distribution in the liquid follows $p(z) = p_a - \gamma\kappa_t z/h$, the curvature of the meniscus at z is $\kappa(z) = \kappa_t z/h$, implying that the curvature of the interface open to the atmospheres increases with the height, as depicted in Fig. 1(b). To describe the average velocity of the viscous flow through a conduit of varying cross-sectional area, we employ Darcys law [19,20]:

$$u = -\frac{k}{\mu}\frac{\partial(p + \rho g z)}{\partial z},\tag{2}$$

where k is the permeability, ρ the liquid density, μ the liquid viscosity, and g the gravitational acceleration. Integrating Eq. (2) with respect to z from 0 to h, we get $\mu\int_0^h (u/k)dz = \gamma\kappa_t - \rho g h$.
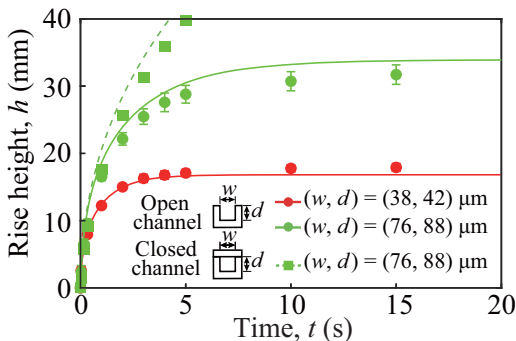
FIG. 4. Experimental (symbols) and theoretical (lines) results of the rise height of ethanol versus time, in vertical closed and open channels with $(w, d) = (38, 42)$ μm and $(76, 88)$ μm. A broken line is a theoretical result assuming no evaporation. Solid lines are theoretical results with the evaporative flux over the side open area given by $J' = J_0 w^{0.38}$.

Using Eq. (1), we get a nonlinear differential equation for h:

$$\dot{h} = \frac{1}{\mu A(h) I_1(h)} \{\gamma \kappa_t - \rho g h - \mu J'[h I_1(h) - I_2(h)]\}, \tag{3}$$

where $I_1(h) = \int_0^h A^{-1}(z) k^{-1}(z) dz$ and $I_2(h) = \int_0^h z A^{-1}(z) k^{-1}(z) dz$. As the permeability is proportional to the cross-sectional area of flow, we write $k(z) = k(0) A(z)/A(0)$, where $A(0) = wd$. The permeability of an open rectangular microchannel [21] with $\theta = \pi/2$ at $z = 0$ is given by $k(0) = (w^2/12)\{1 - \sum_{m=\text{odd}}^{\infty} 96 w [\tanh(m\pi d/w)]/(m^5 \pi^5 d)\}$.

We numerically integrate Eq. (3) to compute the temporal evolution of the rise height of liquid. Figure 4 shows the computational and experimental results of capillary rise dynamics in channels with $(w, d) = (76, 88)$ μm and $(38, 42)$ μm. We first see that the liquid rise in the former channel with one side open (green circles) is severely limited as compared to the rise in the channel with all the four sides closed (green squares). The broken line corresponds to the computational result assuming no evaporative flux, $J' = 0$. Our model (solid line) considering the evaporative flux, $J' = J_0 w^{0.38}$, agrees with the experimental data for the open channel. In particular, it correctly captures the early saturating behavior of the rise height caused by evaporation.

We note in Fig. 4 that the final rise height of the wider open channel (green circles) is greater than that of the narrower open channel (red circles) unlike nonevaporative capillary rise where narrower ones always result in greater equilibrium rise height. It is because the enhanced evaporative mass loss offsets the strong capillary effects in narrower channels. Below we further quantify the evaporation effects on capillary rise in the context of the equilibrium rise height.

The equilibrium rise height, h_e, is obtained by letting $\dot{h} = 0$ in Eq. (3) once the width and depth of a rectangular channel are given. Figure 5(a) displays the contour map of h_e as both w and d range from 0 to 0.5 mm. We plot the theoretically obtained h_e as a function of the channel depth d at fixed widths in Fig. 5(b). It is seen that h_e increases steeply with the increase of d when d is small, but it plateaus when d gets large. In Supplementary Material B [17], we show $h_e = \gamma[2\cos\theta_e/w - (1 - \cos\theta_e)/d]/(\rho g)$, where θ_e is the equilibrium contact angle, without evaporation. This reduces to $h_e = 2\gamma/(\rho g w)$ when $\theta_e = 0$, which corresponds to the asymptotic dashed lines in Fig. 5(b). In the small d regime, the evaporative loss from the open surface can be compensated more effectively as d increases, resulting in the steep increase of h_e with the increase of d. When the channel is sufficiently deep, the evaporative loss is insignificant compared with the amount of liquid pumped upward by capillarity.
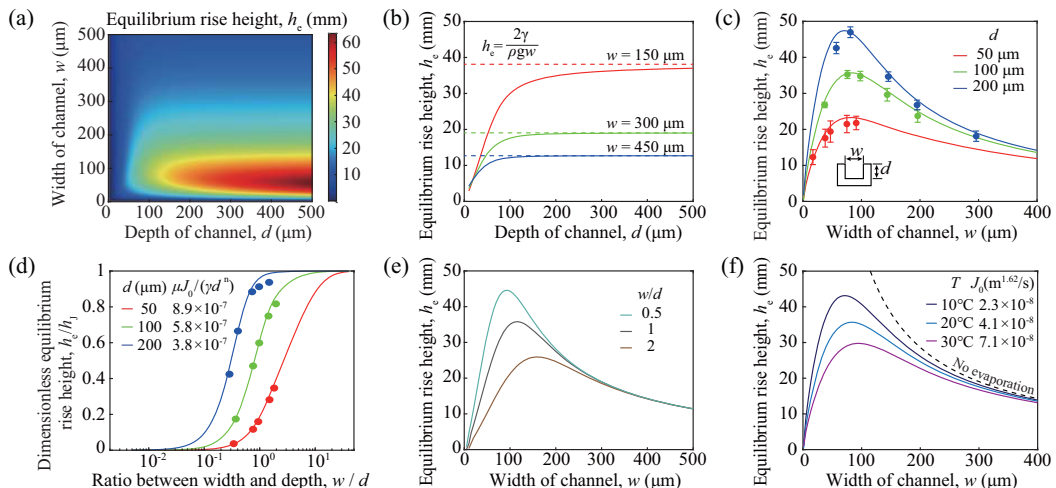
FIG. 5. (a) The contour map of the equilibrium capillary rise height of ethanol, h_e, in open rectangular channels. (b) h_e versus channel depth, d, for different channel widths, w. (c) h_e versus w for different d. (d) Dimensionless height h_e/h_J versus $w/$d for different values of $\mu J_0/(\gamma \mathrm{d}^n)$. (e) h_e of open rectangular channels with different depth-to-width ratios. (f) h_e versus channel width for different J_0. All the results are from numerical computations except for circular symbols in (c) and (d) which are from experimental measurements.

In Fig. 5(c) that plots h_e versus w for fixed values of d, we find an optimal channel width to exist that maximizes h_e at given d. When w is smaller than the optimal width, h_e increases with w because the ratio of the evaporative flux ($\sim h w^{1-n}$) to the liquid volume ($\sim \mathrm{d}wh$), $\sim w^{-n}/$d, is higher for a narrower channel. However, for w greater than the optimal width, h_e decreases with w due to combined effects of the excessive evaporative loss and the decreased capillary effects. Therefore, the evaporative effects are the most pronounced in the small w region where h_e increases with w rather than decreasing.

We note that Fig. 5(c) can be replotted for a dimensionless rise height, as shown in Fig. 5(d). Because h_e is a function of w, d, ρg, σ, μ, and J_0, dimensional analysis reveals that the dimensionless height h_e/h_J, with the Jurin height $h_J = 2\gamma/(\rho g w)$, depends on the two dimensionless variables: $w/$d and $\mu J_0/(\gamma \mathrm{d}^n)$. We see in Fig. 5(d) that h_e/h_J is indeed determined by $w/$d when a value of $\mu J_0/(\gamma \mathrm{d}^n)$ is given. Although this dimensionless plot elegantly displays the complete functional dependence of the equilibrium rise height, it is hard to find the optimal channel dimension to maximize the rise height.

Figure 5(e) plots h_e for channels with $w/$d $= 0.5$, 1, and 2, revealing that the optimal width to maximize h_e for a given aspect ratio is greater for a shallower channel. Namely, the optimal width is 93, 116, and 160 μm for $w/$d $= 0.5$, 1, and 2, respectively. This is because evaporation effects are more significant for shallower channels (larger $w/$d), and thus the width range is broadened, where the rise height increases with w.

In addition to the channel dimensions, the strength of evaporation denoted as J_0 plays an important role in determining h_e. As the ethanol temperature varies from $10\,^\circ$C to $30\,^\circ$C, J_0 was numerically calculated to change from 2.3×10^{-8} to 7.1×10^{-8} m$^{1.62}$ s^{-1} with the saturation concentration c_s assumed to follow the ideal gas behavior: $c_s = MP_s/(RT)$. Here M, P_s, and R are the molecular weight, the saturation vapor pressure and the gas constant, respectively. Figure 5(f) plots the theoretically predicted h_e for a channel with d $= 100$ μm as a function of the width at different values of J_0. We see that the maximum h_e for $J_0 = 2.3 \times 10^{-8}$ m$^{1.62}$ s^{-1} is 1.45 times greater than that for $J_0 = 7.1 \times 10^{-8}$ m$^{1.62}$ s^{-1}. However, the effects of J_0 on h_e become less

significant for excessively large w because the small rise height due to reduced capillary effect and enhanced gravitational force for large w limits the area where evaporation occurs. Overall, the effects of evaporation are found to be important when the channel width and depth are smaller than ~200 μm for ethanol.

In summary, we have investigated the capillary rise dynamics of an evaporative liquid in a vertical open microchannel using a combination of experiment and theory. We have evaluated the evaporation rate per channel length as a function of the channel width, to find that the rate depends only weakly on the width owing to the enhanced evaporation near the solid-liquid-gas contact line. We have derived a differential equation for the temporal evolution of the rise height, by incorporating the quantified evaporation rate in the mass conservation equation while employing the concept of permeability to account for the varying cross-sectional area of the liquid column. The experimental measurement results of the capillary rise dynamics that are limited by evaporation have been shown to be in good agreement with our theoretical prediction. A remarkable feature of the evaporative capillary rise is that there exists an optimal channel width that maximizes the equilibrium rise height once the channel depth is given, unlike nonevaporative rise whose equilibrium height monotonically increases with reduction of channel width.

The theoretical model constructed here can lay a foundation for understanding the evaporative capillary rise dynamics occurring in porous media including wet rocks, bricks, bread, and paper, as well as simple open channels adopted in coolers of heating, ventilation, and air-conditioning equipment [22]. Furthermore, the subtle dependence of the capillary rise distance on the combination of depth and width of channel leads us to think about its physical implication on the design principles of deep skin wrinkles of some animals. The water transported in the skin wrinkles of elephants has been reported to help them cool their body [23], so that both wide water coverage of their skin and effective evaporation are important. Desert lizards draw water from wet soil by using skin wrinkles that act as capillary channels up to their mouths [24]. In this case, suppressing evaporation while maximizing the flow rate would be a primary objective function. Our work can be a starting point to elucidate such biological capillary channel designs as well as help us design optimal fluid networks relying on both evaporation and capillarity.

[1] P.-G. de Gennes, F. Brochard-Wyart, and D. Quéré, *Capillarity and Wetting Phenomena: Drops, Bubbles, Pearls, Waves* (Springer, New York, 2004).

[2] A. Faghri, Review and advances in heat pipe science and technology, J. Heat Transf. **134**, 123001 (2012).

[3] Q. Wang, N. Li, B. Bolto, M. Hoang, and Z. Xie, Desalination by pervaporation: A review, Desalination **387**, 46 (2016).

[4] N. S. Lynn and D. S. Dandy, Passive microfluidic pumping using coupled capillary/evaporation effects, Lab Chip **9**, 3422 (2009).

[5] E. Reyssat and L. Mahadevan, Hygromorphs: From pine cones to biomimetic bilayers, J. R. Soc. Interface **6**, 951 (2009).

[6] C. N. Kaplan and L. Mahadevan, Evaporation-driven ring and film deposition from colloidal droplets, J. Fluid Mech. **781**, R2 (2015).

[7] N. Fries, K. Odic, M. Conrath, and M. Dreyer, The effect of evaporation on the wicking of liquids into a metallic weave, J. Colloid Interface Sci. **321**, 118 (2008).

[8] N. S. Achour, M. Hamdaoui, and S. Ben Nasrallah, Wicking and evaporation of liquids in knitted fabrics: Analytic solution of capillary rise restrained by gravity and evaporation, Int. J. Mech. Mechatron. Eng. **9**, 1387 (2015).

[9] M. Liu, J. Wu, Y. Gan, D. A. H. Hanaor, and C. Q. Chen, Tuning capillary penetration in porous media: Combining geometrical and evaporation effects, Int. J. Heat Mass Transf. **123**, 239 (2018).

[10] C. van Engeland, B. Haut, L. Spreutels, and B. Sobac, Evaporation versus imbibition in a porous medium, J. Colloid Interface Sci. **576**, 280 (2020).

[11] Y. A. Çengel, *Heat Transfer: A Practical Approach* (McGraw–Hill, New York, 2003).

[12] R. D. Deegan, O. Bakajin, T. F. Dupont, G. Huber, S. R. Nagel, and T. A. Witten, Capillary flow as the cause of ring stains from dried liquid drops, Nature (Lond.) **389**, 827 (1997).

[13] G. Berteloot, C.-T. Pham, A. Daerr, F. Lequeux, and L. Limat, Evaporation-induced flow near a contact line: Consequences on coating and contact angle, Europhys. Lett. **83**, 14003 (2008).

[14] E. Rio, A. Daerr, F. Lequeux, and L. Limat, Moving contact lines of a colloidal suspension in the presence of drying, Langmuir **22**, 3186 (2006).

[15] G. Berteloot, A. Hoang, A. Daerr, H. P. Kavehpour, F. Lequeux, and L. Limat, Evaporation of a sessile droplet: Inside the coffee stain, J. Colloid Interface Sci. **370**, 155 (2012).

[16] R. D. Deegan, O. Bakajin, T. F. Dupont, G. Huber, S. R. Nagel and T. A. Witten, Contact line deposits in an evaporating drop, Phys. Rev. E **62**, 756 (2000).

[17] See the Supplementary Material at http://link.aps.org/supplemental/10.1103/PhysRevFluids.7.L032001 for details of numerical solutions and derivations of equilibrium capillary rise height.

[18] M. M. Weislogel, Compound capillary rise, J. Fluid Mech. **709**, 622 (2012).

[19] M. Reyssat, L. Courbin, E. Reyssat, and H. A. Stone, Imbibition in geometries with axial variations, J. Fluid Mech. **615**, 335 (2008).

[20] J.-B. Gorce, I. J. Hewitt, and D. Vella, Capillary imbibition into converging tubes: Beating Washburn's law and the optimal imbibition of liquids, Langmuir **32**, 1560 (2016).

[21] P. J. P. de Leon and L. F. Velásquez-García, Optimization of capillary flow through open-microchannel and open-micropillar arrays, J. Phys. D: Appl. Phys. **49**, 055501 (2016).

[22] P. M. Cuce and S. Riffat, A state of the art review of evaporative cooling systems for building applications, Renew. Sust. Energ. Rev. **54**, 1240 (2016).

[23] A. F. Martins, N. C. Bennett, S. Clavel, H. Groenewald, S. Hensman, S. Hoby, A. Joris, P. R. Manger, and M. C. Milinkovitch, Locally-curved geometry generates bending cracks in the African elephant skin, Nat. Commun. **9**, 3865 (2018).

[24] W. C. Sherbrooke, *Introduction to Horned Lizards of North America* (University of California Press, Oakland, CA, 2003).